Influence of impulse voltage repetition frequency on RPDIV in partial vacuum

Influence of Impulse Voltage Repetition Frequency on RPDIV in Partial Vacuum

Doris Ragna Meyer
High Voltage Laboratory, Swiss Federal Institute of Technology, ETH Zürich
ETL H 26, Physikstrasse 3
8092 Zurich, Switzerland

Andrea Cavallini and **Luca Lusuardi**
Lab. Innovazione Tecnologica, University of Bologna
Viale Risorgimento 2
40136 Bologna, Italy

Davide Barater, Giorgio Pietrini and **Alessandro Soldati**
Department of Information Technology, University of Parma, Italy
Parco Area delle Scienze, 181/a
43124 Parma, Italy

ABSTRACT

The reliability of low-voltage inverter-fed motors is highly dependent on the inception of partial discharges. The effect of impulsive waveform parameters must be investigated to predict the repetitive partial discharge inception voltage (RPDIV) and define test procedures that can indicate properly the behavior in service of the insulation system. This paper focuses on the RPDIV of magnet wires using twisted pairs subjected to repetitive unipolar impulsive voltage waveforms. The effects of supply frequency (5 to 200 kHz) at pressure levels that are typical for aircraft (20 to 100 kPa) is examined. Results show that RPDIV steadily decreases with frequency up to 100 kHz where it reaches a plateau. This behavior is explained as an effect of the oscillations that inevitably exist in the applied voltage waveform. Therefore, a conservative estimate of the RPDIV could be achieved by raising the supply frequency well above the operation frequency. In the experiments, the RPDIV is decreasing linearly with pressure. If this behavior could be confirmed for other insulation systems, the design of systems working at pressures typical of aircraft would result relatively easy.

Index Terms –**Electrical insulation, partial discharges, PDIV, RPDIV, inverter-fed machines.**

1 INTRODUCTION

THE electrification of traction/propulsion systems is making its way in all fields of transportation. In the automotive and aviation sector, two significant challenges can be foreseen for insulation systems: the gradual introduction of wide bandgap (WBG) devices [1], and the operation of actuators in a partial vacuum [2].

WBG devices are extremely promising since their short rise times (or large slew rates) enable better control strategies and reduce commutation power losses. However, because of the mismatch between the motor and the cable (connecting the motor to the inverter) overvoltages between 2-3 times the DC bus voltage can appear at the motor terminals during the surge flanks [3]. Due to the partly inductive, partly capacitive nature of the winding, these overvoltages are applied to the turns in proximity of the line terminals. The shorter the rise time, the larger is the probability of large overvoltages and the voltage drop on the first turns of the winding. In a random wound motor, when the first and last turns of the coil are in contact, the voltage across the turn insulation can reach 90% of the so-called jump voltage [4]. This situation can be mitigated using hairpin (form wound) windings. However, the larger slew rates support high turn voltages, even using stators manufactured through the hairpin technology [5]. Moreover, electric vehicles and aircraft insulation must be able to operate satisfactorily in a partial vacuum (residual pressures are 50 kPa and 20 kPa for electric vehicles and airplanes, respectively), where the breakdown strength of the air is lower than that at ground level.

Manuscript received on 31 March 2017, in final form 13 February 2018, accepted 13 February 2018. Corresponding author: A. Cavallini.

Thus, there is a concrete risk that partial discharges (PD) are incepted in the insulation system, turning WBG inverters into an issue for insulation designers.

To avoid that an opportunity becomes a problem, it is important to quantify how the use of WBG inverters can favor PD inception in a motor stator. Besides understanding the physics of the process, it should be understood whether the qualification procedures proposed by the IEC 60034-18-41 [4] for industrial motors can ensure the reliability of actuators subjected to extreme voltage waveforms and ambient conditions. The standard supports, in fact, the use of sinusoidal waveforms to determine whether insulation models are PD free or not and does not provide provisions for motors working in a partial vacuum.

This paper describes tests that were performed in a partial vacuum using a SiC pulse generator able to produce surges having a rise time of 14 ns, with carrier frequency up to 200 kHz. The goal is to start to establish the empirical basis to derive criteria for the design of reliable insulation systems to prevent PD inception in WBG actuators used in a partial vacuum environment. This paper does not address issues as the effect of extreme ambient conditions (e.g., high/low temperature) on PD inception.

2 EXPERIMENTAL SET-UP

2.1 TEST OBJECTS

Twisted pairs were used in all tests. The manufacturing procedure was the following. The insulation at both ends of 15 cm long wires was removed with a blade. Then, the ends were fastened to the measurement platform and twisted for ten complete turns.

To estimate the permittivity of the insulation (used for modeling RPDIV, see Appendix A), the geometry of the wire was measured first. The wire has an outer diameter of 625 μm ± 4 μm and an insulation thickness of 28 μm ± 2 μm. The outer diameter was measured using a micrometer 25 mm in range, with an accuracy of 1 μm. The insulation was removed by burning the insulation with a Bunsen burner and then applying a solvent (hydrochloric acid ≥ 37% UN1789 SIGMA-Aldrich). Then, the bare conductor diameter was measured using the same micrometer. It is important to observe that, since the thickness is obtained calculating the difference of two quantities much larger than the thickness itself, it is necessary to reduce the variance of the measurements by averaging. Thus, the thickness was estimated by averaging results from 20 samples. Failure to do the above can easily provide meaningless results when the dielectric permittivity needs to be estimated.

To measure the real part of the insulation permittivity, the capacitance of a 10 cm wire splice was measured as a function of frequency by a High-Resolution Dielectric Analyzer (Novocontrol Technologies Alpha-N). For this purpose, the insulation coating of the wire was removed at both ends, while the middle part was painted with conductive paint to create the ground electrode.

The values for the capacitance were then used to calculate the real part of the permittivity ε_r according to:

$$\epsilon_r = \frac{C_p \cdot \log(d_{out}/d_{in})}{2\pi\varepsilon_0 l}, \quad (1)$$

where C_p, d_{out}, d_{in}, ε_0 and l are the measured capacitance, the outer diameter, the inner diameter, the vacuum permittivity and the length of the wire, respectively. Based on the average value recorded over 10 samples, permittivity data are presented in Table 1 along with their 95% confidence intervals.

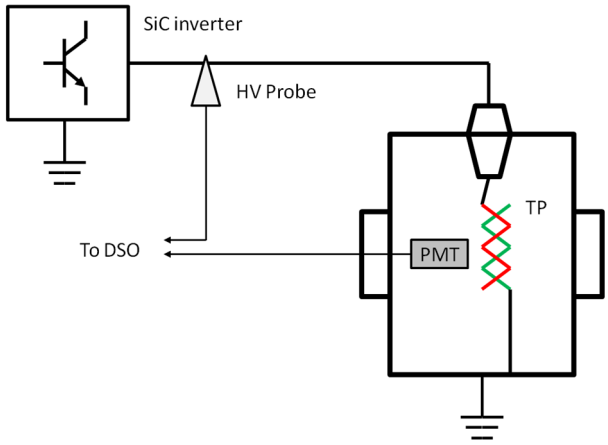

Figure 1. Test circuit (TP: Twisted Pair, PMT: Photomultiplier Tube).

Table 1. Results of the measurements of relative permittivity.

Frequency (kHz)	Relative permittivity with 95% confidence interval
5	4.54 [4.21 - 4.87]
10	4.51 [4.19 - 4.84]
25	4.47 [4.14 - 4.79]
50	4.42 [4.10 - 4.75]
75	4.40 [4.08 - 4.72]
100	4.38 [4.06 - 4.69]
200	4.32 [4.07 - 4.57]
500	4.27 [4.02 – 4.52]

RPDIV tests were carried out at 100 kPa, 65 kPa, and 20 kPa and for the frequencies 5 kHz, 10 kHz, 25 kHz, 50 kHz, 75 kHz, 100 kHz and 200 kHz. RPDIV is defined as the voltage level at which the probability of incepting a PD per voltage surge is equal to 50%. Indeed, during the test, the inception of the first PD gave rise to a continuous activity (PD on both the rising and falling flanks of the surges) given the large repetition frequency of the voltage impulses. For each test condition, RPDIV was measured on 10 different samples. The twisted pair under test was replaced after each measurement to prevent the influence of PD-induced degradation on experimental results. A sealed steel tank with four openings was used to carry out measurements in a partial vacuum. A Speedivac ED75 pump is used to achieve the desired vacuum level.

2.2 TEST CIRCUIT

The circuit shown in Figure 1 was used to detect PDs.The test circuit was fed by a SiC pulse generator connected to a DC power source. The SiC pulse generator is programmable to different supply frequency levels and was manufactured by the MEltIng laboratory of the University of Parma (Italy). Measurements up to

200 kHz are possible. The square wave voltage is positive unipolar, and the voltage impulses have a rise time of about 14 ns (at no load).

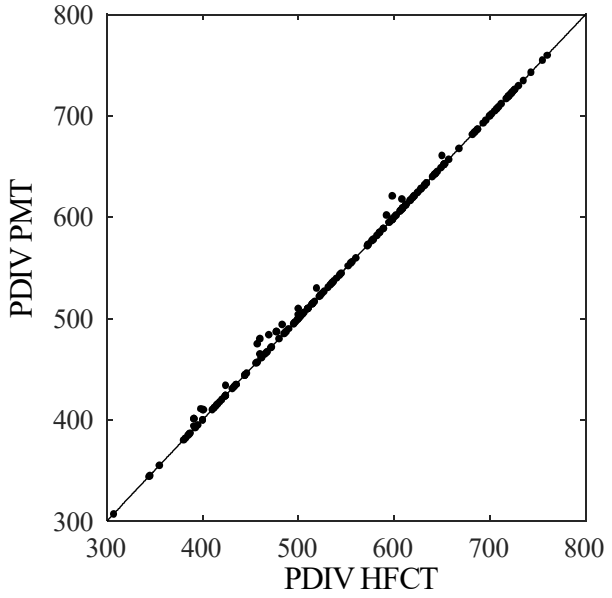

Figure 2. PDIV RMS values detected with PMT compared to HFCT. PDIV values were obtained with pressures of 100 kPa, 65 kPa and 20 kPa, testing different wire types with insulation thickness ranging from 10 to 50 μm.

Overshoots at voltage flanks are considered by measuring the peak-to-peak voltage $U_{pk\text{-}pk}$ using a high voltage probe (Tektronix P6015A, 75 MHz bandwidth, 3 pF) and an oscilloscope (Tektronix DPO 5034). Due to space limitation in the test tank, during the tests the voltage probe was connected to the SiC pulse generator output. Thus, before starting the tests, the high voltage at the sample terminal was measured with the tank open using an additional probe. A mapping of the voltage difference between the two terminals was evaluated and (during the tests) the measured voltage values were corrected.

2.3 PD DETECTION

The most common PD detection systems couple the conducted PD pulse currents to achieve an estimate of apparent charge [6]. However, under square voltage waveforms, PD often occur during the voltage turn on (off) [7], when the disturbance associated with the voltage source operation can mask the PD signal. With surges having rise times of the order of tens on ns, comparable with the time duration of a PD pulse [8], the separation of PD signal from inverter interference is often problematic. For these reasons, PD detection under inverter surges is usually achieved through UHF systems [9] [11] or, alternatively, using optical systems as e.g. Photo-Multiplier Tubes, PMTs [12]. For this study, considering the extremely large slew rate of the SiC pulse generator and the fact that the tests were performed in a sealed tank, we decided to use an optical system. A PMT Module H5773-04 from Hamamatsu was inserted in the test cell. An envelope demodulator in series with an amplifier was connected directly to the PMT to raise the signal-to-noise ratio. The amplified signals were eventually sent to an oscilloscope using an additional high pass filter.

To test the sensitivity of the optical system, tests were carried out using AC sinusoidal voltages comparing the PDIV values obtained from the optical system with those obtained using a HFCT connected directly to the bushing (thus using the bushing and cable stray capacitances as coupling capacitors). The HFCT was connected to a commercial PD detector (TechImp PDBase II system). The results obtained from these preliminary tests allow to conclude that the PMT is almost as sensitive as the HFCT (see Figure 2).

It is important to observe that detection under surges provided by large slew rate pulse generators using PMTs does not allow to measure as accurately the PDIV as under AC waveforms. As a matter of fact, shielding perfectly the PMT from the SiC pulse generator interference proved to be impossible. The PMT was enclosed in a grounded metallic case together with the envelope demodulator and the amplifier, and connected to the external oscilloscope via a BNC cable with double screen. However, a circular hole (∅=10 mm, comparable to the PMT photocathode size) had to be drilled in the case to let in the light. Although this hole was not very large, capacitive coupling between the currents flowing in the test cell and the elements inside the case occurred at voltage surge flanks. Since the frequency content of the surges was comparable with that of the PD (under AC, we could determine that the optical pulse lasts around 8 ns), PDIV could be detected when the SiC pulse generator interference (almost deterministic) started to display randomly superposed signals. Therefore, PDIV was often recorded at the voltage level at which recurring PD took place. This way, not the PDIV is detected, but the repetitive partial discharge inception voltage (RPDIV) [4].

2.4 EXPERIMENTAL PROCEDURE AND DATA VARIANCE

To determine the RPDIV, the voltage was increased in steps of 10 V starting at a value high enough to avoid excessively long test times, but lower than the RPDIV (about 70% of the expected RPDIV).

Using sinusoidal voltage waveforms, we observed that PDIV confidence intervals increase as pressure decreases [13]. This behavior can be explained bearing in mind that photoionization of gas molecules provides initiatory electrons to trigger PD. At low pressures, given the reduced number of gas molecules per unit volume, the mean time between two consecutive starting electrons (MTBE) should increase. According to [14], the MTBE should scale as:

$$MTBE(p) = MTBE(p_0) \cdot p_0/p \qquad (2)$$

To tackle this problem, the voltage was ramped up in steps having a pressure-dependent duration i.e. 30 s at 100 kPa, 60 s at 65 kPa and 90 s at 20 kPa (note: the durations do not strictly follow Equation (2) to limit the test times).

During all measurements, the relative humidity of air varied between 25% and 50% and the ambient temperature was between 18 and 25°C.

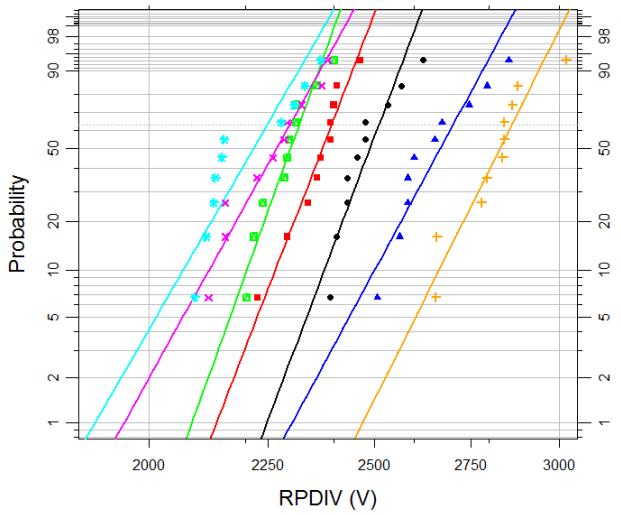

Figure 1. Weibull chart of measured RPDIV peak-to-peak values at 100 kPa remaining pressure at 5kHz (orange +), 10kHz (blue ▲), 25kHz (black ●), 50kHz (red ■), 75kHz (green □), 100kHz (pink x) and 200kHz (cyan *).

3 RESULTS

Figures 3-5 show the measured data fitted to Weibull distribution for all frequencies at 100 kPa, 65 kPa and 20 kPa, respectively. A few outliers were discarded for the determination of the distribution. Censored data is highlighted by a square box in Figure 4. The Weibull shape parameters are reported in Table 2 for all test conditions.

Table 2. Summary of Weibull shape parameters for the plots in Figures 3-5.

Frequency	100 kPa	65 kPa	20 kPa
5 kHz	31.2	20.9	9.2
10 kHz	28.9	17.5	9.9
25 kHz	41.5	16.3	30.8
50 kHz	40.3	12.2	55.1
75 kHz	43.4	14.0	19.9
100 kHz	28.0	14.1	18.4
200 kHz	27.0	15.2	21.6

It is interesting to observe that, for 100 kPa and 65 kPa, data points align with similar slopes. For 20 kPa, experimental data can be grouped based on the supply voltage frequency. The following groups can be observed:

- Data measured with a supply frequency of 5 kHz and 10 kHz, which display low β values (9-10).
- Data measured with a supply frequency of 25 kHz and 50 kHz, with higher β values (30-55).
- Data measured with higher supply frequencies, with intermediate β values (18-21) and a downward curvature hinting a threshold value.

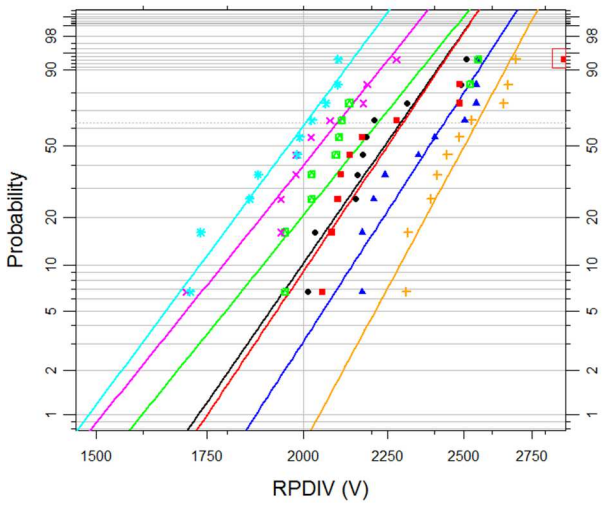

Figure 2. Weibull chart of measured RPDIV peak-to-peak values at 65 kPa remaining pressure at 5kHz (orange +), 10kHz (blue ▲), 25kHz (black ●), 50kHz (red ■), 75kHz (green □), 100kHz (pink x) and 200kHz (cyan *)

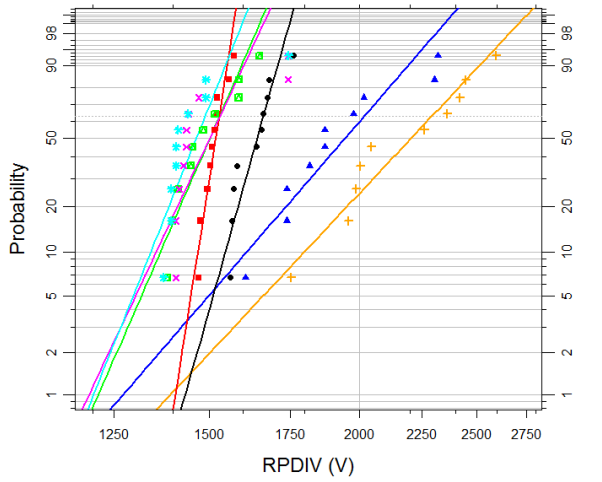

Figure 3. Weibull chart of measured RPDIV peak-to-peak values at 20 kPa remaining pressure at 5kHz (orange +), 10kHz (blue ▲), 25kHz (black ●), 50kHz (red ■), 75kHz (green □), 100kHz (pink x) and 200kHz (cyan *)

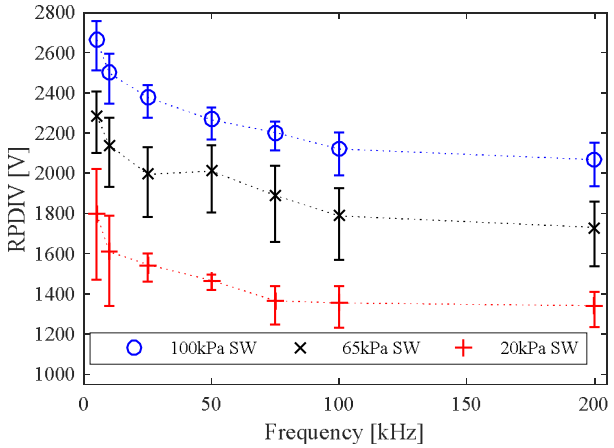

Figure 4. RPDIV ($V_{pk\text{-}pk}$) 10th percentile (B10) as a function of frequency and pressure.

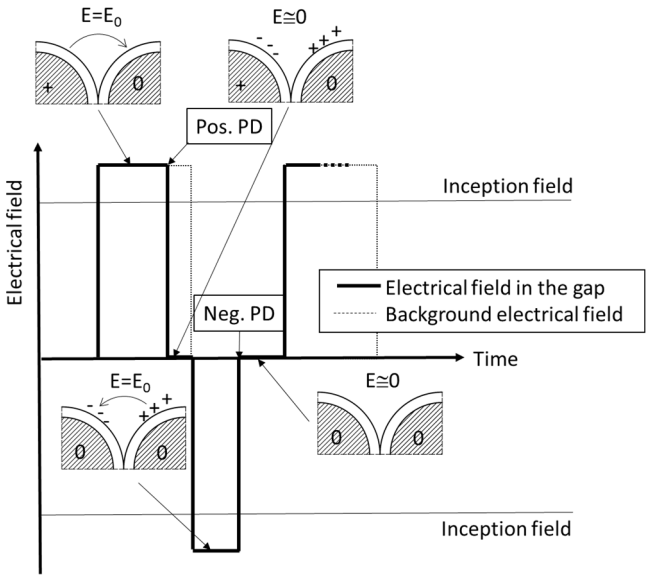

Figure 5. Partial discharge under unipolar waveforms.

Figure 6 shows the peak-to-peak RPDIV B10 (10% probability percentile) and its 95% confidence intervals as a function of supply frequency for all pressure levels. A low probability percentile was selected to represent RPDIV as it provides indication about the most unfavorable values of RPDIV, which might however be relevant for motor insulation. At all frequencies, the RPDIV decreases with pressure. Also, at all pressure levels, the RPDIV appears to decrease for increasing supply frequency reaching a minimum above 100 kHz. The saturation frequency seems to be a function of pressure (around 100 kHz at 100 kPa and 65 kPa, close to 75 kHz at 20 kPa).

4 DISCUSSION

The discussion of the data casts some problems since we measured using unipolar voltage waveforms. Moreover, since it was impossible to isolate a single PD event from the PMT signal, we report the RPDIV, i.e. the voltage at which the inception of repetitive discharges takes place. Owing to these peculiarities, one has to consider two things. On the one hand, the PDIV is necessarily lower than the value reported here. On the other hand, space charge left by previous PD events plays a non-negligible role. These assumptions are clarified by Figure 7, which shows the electrical field at the discharge site and the corresponding space charge distributions due to PD events. In the Figure, the memory effect due to the space charge left by PD events does not decrease with time. However, charge relaxation might be significant at the lowest frequencies. Unfortunately, measuring space charge evolution within an appropriate period (lower than tens of μs) using electrostatic voltmeters is out of question (moving the electrometer to the discharge site takes much longer than a few ms, the electrometer itself has a time constant much longer). Indeed, we observed indirectly that memory effect can be considered almost perfect above 10 kHz [15]. Having clarified the possible limitations, it is feasible to comment the results.

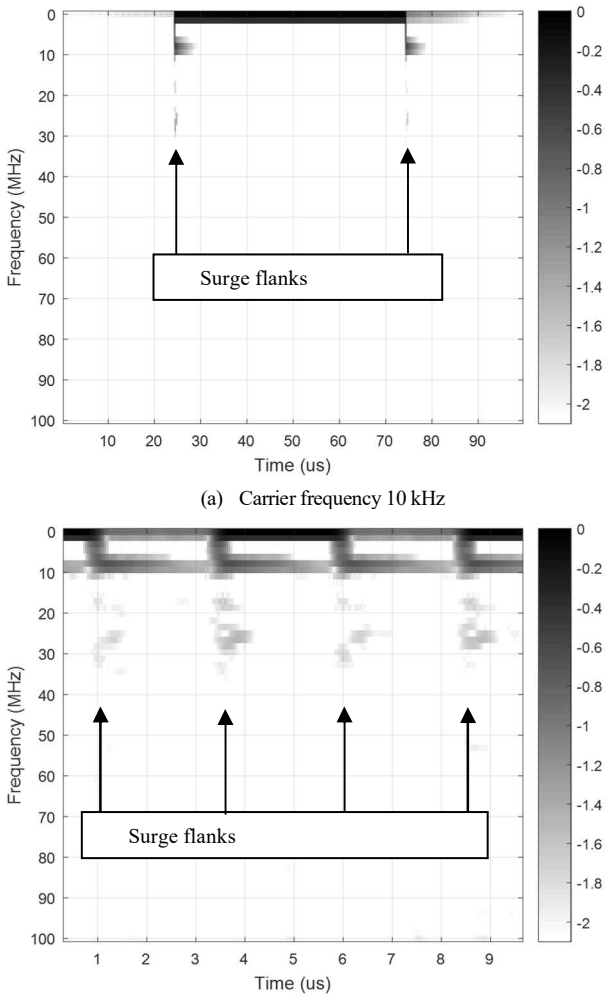

(a) Carrier frequency 10 kHz

(b) Carrier frequency 200 kHz

Figure 6. Short-Time Fourier Transform of the repetitive surges applied to the twisted pairs.

4.1 INFLUENCE OF SUPPLY FREQUENCY ON RPDIV

Figure 6 highlights a clear dependence of RPDIV on supply frequency. At all pressure levels, the RPDIV decreases for increasing frequency, although it reaches a plateau for frequencies higher than 100 kHz. At the lowest frequencies (5-20 kHz), this phenomenon is explained by the PD space charge, for the reasons exposed above. However, above these frequencies, an alternative explanation is needed.

The dependence on frequency seems in agreement with the findings of Pfeiffer, and Paede [16], who performed measurements on twisted pairs. However, they used sinusoidal voltages and a much wider frequency range (between 50 Hz and 3 MHz). They explain the differences in the observed PDIV values resorting to the behavior of relative permittivity. However, the changes in the permittivity that we measured in the frequency range 0-500 kHz (see Table 1) are not sufficient to support this claim (simple calculations assuming uniform field between covered electrodes show that the field might increase of a few percent).

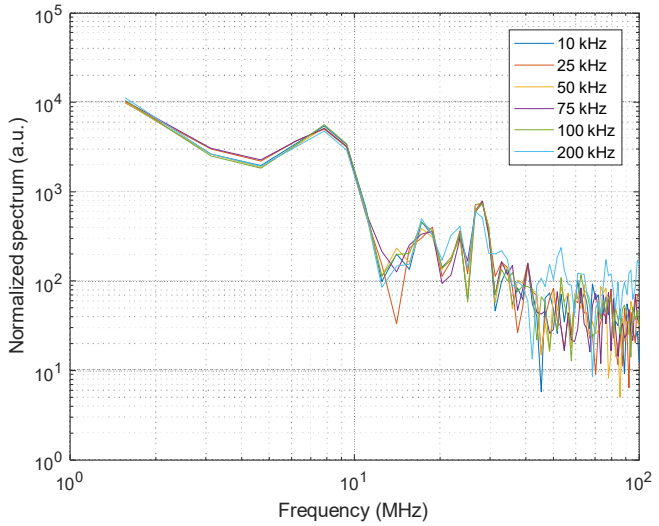

Figure 7. Spectra having the largest frequency content for the various values of carrier frequency.

Furthermore, it is worthwhile to understand how frequency can be defined for repetitive square waves. In fact, one could consider the carrier frequency (e.g., 200 kHz) or, alternatively, the instantaneous frequency. Focusing on the latter, the largest instantaneous frequency can be found in correspondence of the square wave fronts and might have an impact on the permittivity of the dielectric thus on the instantaneous voltage. For this reason, the frequency content of the high voltage surges was investigated using the Short Time Fourier Transform, [17]. As an example, Figure 8 shows the instantaneous spectrum of the applied voltage waveforms for carrier frequencies of 10 kHz and 200 kHz. From a visual inspection of Figure 8, it comes out that surge flanks have the largest frequency content which, however, does not seem to be affected significantly by the carrier frequency.

To obtain a better picture, from each instantaneous spectrum we extracted that with largest equivalent bandwidth [18], i.e., the spectrum defined as:

$$S_{\max}(f) = \max_{t} \int_{0}^{\infty} f \cdot |S(t,f)| \cdot \mathrm{d}f \qquad (3)$$

where f is the frequency, S is the instantaneous spectrum obtained from the STFT algorithm. The results of this procedure are presented in Figure 9, which confirms that the differences between the spectra obtained at the different carrier frequencies are negligible. This evidence proves that the dependence of RPDIV on the carrier frequency is not ascribable to the different instantaneous frequency content of the applied voltage surges (which is related to the rise time).

A more plausible explanation comes from observing the voltage waveforms reported in Figure 10. The Figure shows that the oscillations after the turn on/off of the voltage source have a much different impact at 10 kHz compared with 200 kHz. In particular, comparing the exceeding probability of the voltage absolute values for all carrier frequencies (see Figure 11), it is possible to observe that the highest percentiles increase with the commutation frequencies. Considering that the rate of voltage rise during the test is low but not zero, it is reasonable to assume that, with the same peak voltage, the probability of incepting a PD is larger at 200 kHz than at 10 kHz since for the former waveform the instantaneous voltage exceeds the RPDIV for a longer time.

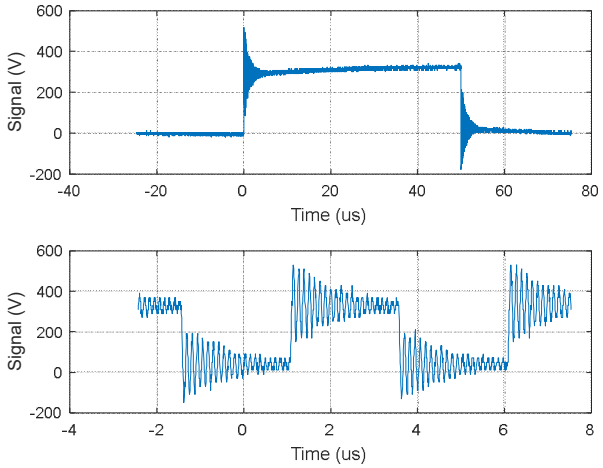

Figure 8. Voltage waveforms for carrier frequency (top) f=10 kHz, (bottom) f=200 kHz.

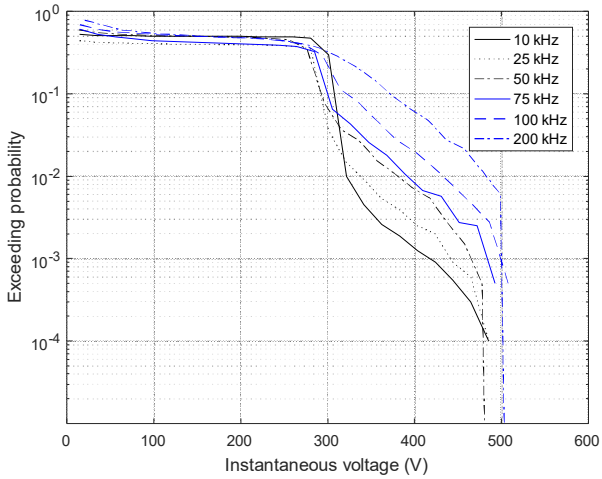

Figure 9. Exceeding probability of the instantaneous voltage (i.e., probability that the instantaneous voltage exceeds a specified value) for the absolute value of different voltage waveforms having the same peak value

An alternative hypothesis that could be invoked to explain the reduction of PDIV (and, consequently, RPDIV) with frequency is that low-magnitude avalanches (glow and pseudo-glow discharges [19]) occur below the sensitivity limit of the detection system. If low-magnitude PD are not detected, the space charge left on the dielectric surface and ions (both positive and negative) in the gap might act as hetero-charge, favoring PD inception.

Assuming that low-intensity PD occur, we can envisage the following scenarios for the space charge associated with these PD:

A. The carriers reach the surface of the insulation, where they are trapped long enough to be still in the discharge

area when polarity reversal occurs. Thus, they might act as hetero-charge favoring PD inception.

B. The avalanche is still growing while polarity reversal takes place. Due to the different mobility of ions and electrons, we can assume (neglecting attachment phenomena) that electrons are on the anode surface, while positive ions are approaching the cathode. The field in the gap can be highly intensified compared to A, easing the development of a streamer avalanche.

To assume that mechanism B is plausible, one should verify that the transit time of the ions is comparable with the half-period of the applied voltage. Thus, the transit times in the discharge gap were estimated assuming N_2^+/N_2 (data for air were not available) and that mobility would remain constant and equal to that at the field corresponding to the DC bus voltage (a conservative assumption). Mobility rates were taken from [20]. The discharge gap length, *d*, was estimated using the procedure discussed in Appendix B. The field was assumed constant in the gap, to simplify the analysis. As Table 3 shows, the transit time becomes comparable with the half-period of the applied voltage when the frequency increases or pressure decreases.

Table 3. Transit times (in per units of the half-period of the applied voltage) of N2+/N2 in the gap.

Frequency (kHz)	100 kPa	65 kPa	20 kPa
5	0.10	0.15	0.24
10	0.19	0.26	0.73
25	0.42	0.61	1.69
50	0.88	1.21	3.39
75	1.17	1.69	4.78
100	1.50	2.08	6.16
200	2.85	3.77	11.95

4.2 INFLUENCE OF PRESSURE ON RPDIV

We start initially with an empirical analysis of the effect of pressure on RPDIV. To do so, we define a quantity that does not need any interpretation model and can serve the purpose of comparing the RPDIV behavior at different frequencies. This quantity is simply the pressure-normalized PDIV, defined as:

$$RPDIV_n(p) = \frac{RPDIV(p)}{RPDIV(100\ kPa)} \tag{4}$$

Figure 12, derived from the data already reported in Figure 6, depicts the behavior of $RPDIV_n$ for the different supply frequencies, as a function of the gas pressure (p). In the range of pressures considered for this work, $RPDIV_n$ decreases linearly with pressure of about 35%. Thus, Figure 12 can be used as a reference to predict the evolution of RPDIV as a function of pressure starting from measurements performed at ground level.

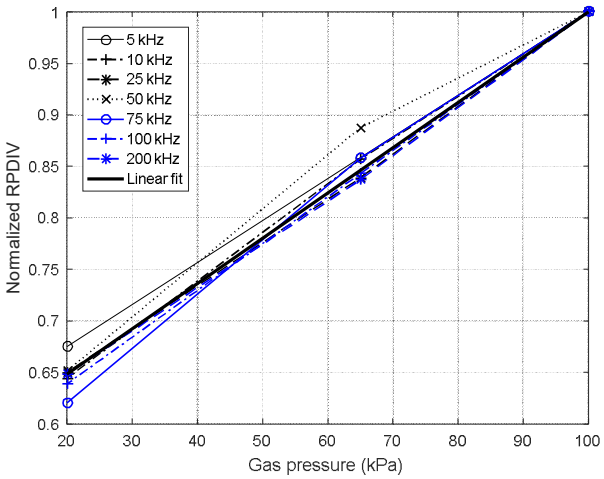

Figure 10. Behavior of normalized RPDIV as a function of gas pressure.

Table 4. Summary of the data used to locate the RPDIV values obtained at 200 kHz on the Paschen curve.

Pressure (kPa)	100	65	20
RPDIV (kV)	1.36	1.11	0.89
Schumann constant (K)	15.0	13.1	11.9
Critical line length (in μm)	49	64	182

To explain the linear behavior of RPDIV in Figure 12, one can refer to the streamer inception criterion proposed by Schumann [21][22], i.e.:

$$\int_0^d \alpha(E/p)\,dx = K \tag{5}$$

where *d* denotes the critical avalanche length, i.e., α is the Townsend effective ionization coefficient at the avalanche head, and E is the electric field. *K* is the Schumann coefficient.

Let us focus on the results obtained at 200 kHz, as the larger number of crests in the voltage surge ensures that the difference between the peak voltage and the actual RPDIV value is the minimum. The Schumann constant and the critical line length were evaluated as explained in Appendix A and reported in Table 4. Assuming that the field is almost uniform (thus $E = RPDIV/d$) eqn. (5) simplifies to $\alpha \cdot d = K$). Negleecting attachment, and referring to the simplified expression of α [23]:

$$\alpha = A \cdot p \cdot \exp\left(\frac{B}{E/p}\right) \tag{6}$$

with A = 11.4 × 10^{-3} ($\mu m^{-1} \cdot kPa^{-1}$), and B = 2.774 × 10^{-4} ($kV\ \mu m^{-1} \cdot kPa^{-1}$). Under the assumptions of uniform field, the exponential term in Equation (6) becomes:

$$\exp\left(\frac{B}{E/p}\right) = \exp\left(\frac{B \cdot p \cdot d}{RPDIV}\right) \tag{7}$$

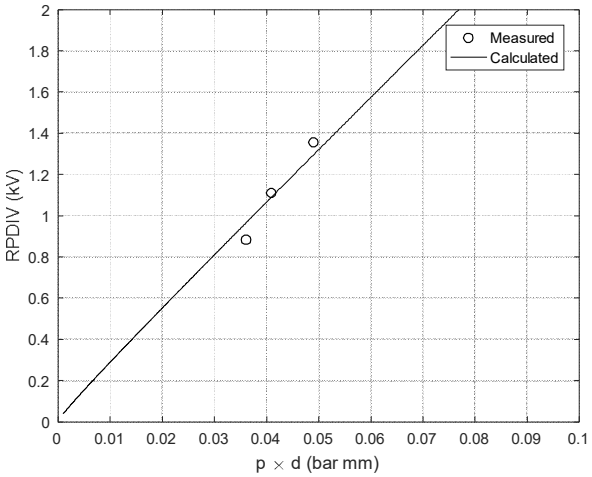

Figure 11. Fitting of RPDIV data via Equation (9). θ =0.48.

Using the data in Table 4, the exponential term ranges from 2.7 to 3.1. Therefore, in a first instance, the variation of the exponential term can be neglected compared with the change of $A \cdot p$, thus justifying the almost linear dependence of RPDIV on pressure. Of course, this simplified analysis neglects the fact that the critical line length changes with pressure and so does K (as shown in Table 4). The latter, is one of the limits of the streamer inception criterion [21]-[24].

Indeed, many authors refer to the Paschen's law as a tool to predict both the PDIV and its dependence on pressure. The Paschen's law expresses the breakdown voltage for gasses between bare metal electrodes creating a uniform field, as a function of the product of pressure and gap length. About the cathode, two conditions might be envisaged, leading to opposite results. On the one hand, one can assume that an insulated cathode does not provide secondary electrons due to positive ion bombardment (which seems the most probable case). On the other hand, above RPDIV, electrons might be trapped on the anode surface, which would become a source of secondary electrons at polarity reversal. In both cases, the condition for breakdown, i.e., the current in the gap goes to infinity due to the positive feedback from the cathode, seems hard to meet. Thus, it is a matter of interest to determine whether the Paschen's law holds true for RPDIV, and under which assumptions.

To model the Paschen curve, we refer to [22]:

$$Vb = \left(\frac{E}{p}\right)_c pd + \sqrt{\frac{C_{elec}}{C_{gas}}}\sqrt{pd} \qquad (8)$$

where $\left(\frac{E}{p}\right)_c$ indicates the minimum electron energy to achieve ionization of the gas molecules, C_{gas} is a constant that depends on the gas type, and C_{elec} accounts for tha nature of the electrode via the probability of emission of secondary electrons from the cathode, γ:

$$C_{elec} = \ln(1 + 1/\gamma). \qquad (9)$$

For air, the constants in eqn. (8) were estimated from data coming from different labs leading to the following simplified equation [23]:

$$V_b = 24.36\,(pd) + 6.72\sqrt{pd}\,. \qquad (10)$$

However, the term multiplying $\sqrt{pd}$ (i.e., the constant 6.72) depends on the electrode nature: an electrode with large emission probability has a lower C_{elec} compared with an electrode with low emission probability. Therefore, we decided to fit the experimental data introducing a fitting constant θ in Equation (11):

$$V_b = 24.36\,(pd) + \theta\sqrt{pd}\,. \qquad (11)$$

The results reported in Figure 13 show that RPDIV data can be measured correctly with a θ=0.48, well below the reference value 6.72. Since $\theta = \sqrt{\ln(1+\gamma^{-1})/C_{elec}}$, values lower than the reference one can be achieved if γ is larger than that of the electrodes used to derive eqn. (11). Although the number of data points is low, this finding seems to indicate that the space charge left by undetected PD events might play a role in RPDIV modeling. However, some approximations were done, and further tests should validate many of them. In conclusion, the Paschen law should be avoided when trying to predict RPDIV values under repetitive surges.

4.3 EFFECT OF MOISTURE IN THE DIELECTRIC

Considering that the moisture within the dielectric can influence RPDIV, we evaluated whether the vacuum levels considered in this work could affect somehow RPDIV by extracting moisture (that could create a drier sample and/or, a wetter gas around the test samples). Therefore, we compared PDIV values obtained from tests carried out on twisted pairs (a) untreated, (b) kept 1 hour at 20 kPa prior testing, and (c) "bone dry" (i.e., dried at 150 °C for 1 hour, following [25]). The results of these tests are reported in Table 5 and show that "bone dry" wires have higher PDIV values than (a) and (b), which provide comparable results. This result implies that the vacuum levels used in our tests are incapable of extracting moisture to a significant extent.

Table 5. PDIV B10 as a function of twisted pair conditioning.

Twisted pair	PDIV [V_{pp}]
Untreated	2046 [1718 - 2274]
Treated 1 hour @ 20 kPa prior testing	2092 [1618 - 2442]
"Bone dry"	2290 [1928 – 2538]

5 CONCLUSION

The data presented in this paper show that rising the commutation frequency might lead to a significant reduction of the estimated RPDIV, something unexpected in the range of commutation frequencies used for this investigation (up to 200 kHz). The phenomenon that more likely explains this behavior is the influence of the oscillations of the supply waveform. The

inception of Townsend discharges below the detection threshold can also be considered, although less convincing evidences (i.e. the large γ value of the "cathode" using the Paschen law) were found.

The effect of reduced pressures seems to be easier to predict, as a linear relationship reproduces with sufficiency accuracy the dependence of RPDIV on pressure. Empirical charts like that reported in Figure 12 need to be evaluated independently by different labs to verify whether a straight line for modeling RPDIV as a function of pressure is applicable in general or not.

If one aims at demonstrating that an aircraft stator is PD free at a cruising altitude 10000-11000 m (corresponding to a pressure of little more than 20 kPa), two conclusions can be derived from these evidences. The first one is that, if possible, testing at a frequency higher than that used by the inverter used in the drive is a conservative choice that should be pursued. The second one concerns the 35% drop of RPDIV from 100 kPa to 20 kPa. If tests have to be performed at ground level, an overvoltage of no less than 35% should be considered.

These evidences suggest that new power modules based on SiC or GaN, with high commutation frequencies, could indeed become an issue for electrical insulation of low voltage actuators. Before arriving to a mass introduction of these devices in the market (especially in aircraft), it would be important to understand better their influence on the reliability of low voltage actuators.

APPENDIX A: EVALUATION OF THE CRITICAL FIELD LINE

To describe PD phenomena, one should bear in mind that Townsend discharges are often below the detection threshold. To model PDIV, reference should be made to streamer inception criteria as that proposed by Schumann [22], i.e.:

$$\int_0^d \alpha(E/p)\,dx = K \qquad \text{(A1)}$$

d denotes the critical avalanche length, i.e., α is the Townsend effective ionization coefficient at the avalanche head, and E is the electric field. K is the Schumann coefficient. The values of α as a function of E/p used in this work were taken from Dutton, where swarm parameters for dry air are tabulated [26].

The bi-dimensional model in Figure A1 (parallel wires) shows the geometry used to model the field in the air surrounding the twisted pairs.

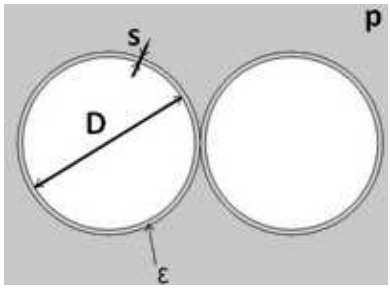

Figure A1. Simplified geometry representing a twisted pair.

To determine d, one must make some considerations. First, we did measure RPDIV, not the PDIV. However, for the highest supply frequencies used in this paper, the space charge from PD events has no time to relax. Thus, as a first approximation, the difference between PDIV and RPDIV can be neglected. Next, one must decide which feature of the applied voltage waveform has to be select to infer the electric field. In the following, we decided to consider the peak voltage.

The last problem to solve is that K depends on d itself [24]. In [21] we found a K value holding for some wires by comparing their PDIV values. Here, this approach is not possible. To get an upper limit for K and d, eqn. (4) was solved in the following iterative way:

1. Set the voltage in the 2D electrode system (Figure A1) to RPDIV, and evaluate the electric field.
2. Set K to a large, unfeasible value.
3. If the integral in eqn. (A1) is lower than K in all field lines, reduce K.
4. Repeat (3) until at least a single field line, of length d, satisfies eqn. (A1) for a lower K value, K^*.

Since a further reduction of K below K^* would ensure that more field lines satisfy eqn. (A1), the critical field line d obtained via this procedure is the upper bound for d.

APPENDIX B: ESTIMATION OF TRANSIT TIMES

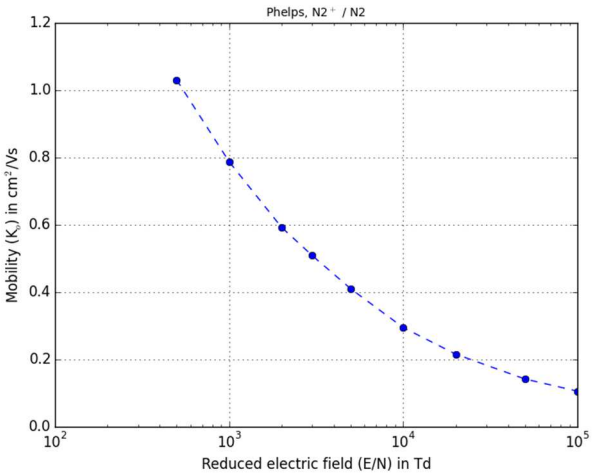

Figure B1. Mobility of N_2^+ ions in N_2 (N_2^+/N_2).

The transit times in the gap between the electrodes were calculated assuming the mobility rates of N_2^+/N_2 from [20] as they appeared to be the lowest for all ions formable in air. For all pressure levels and supply frequencies, the mobility was calculated assuming that the field could be considered constant along the critical field lines:

$$\bar{E} = RPDIV_{peak}/d = RPDIV/(2 \cdot d) \qquad \text{(B1)}$$

In [20], the mobility rate μ_{ion} is given as a function of the reduced electric field (E/N) using Td as the unit (1 Td = 10^{-17} V cm^2), see Figure A1. To determine E/N, we assumed a

constant gas volume and used the ideal gas law setting the temperature to 293 K. Thus, E/N can be expressed as a function of the average field as:

$$\frac{E}{N}\,[V\,cm^2] = 3.11\frac{\bar{E}}{p}\,[V\,cm^{-1}torr^{-1}] \qquad \text{(B2)}$$

Typical values for the ions mobility were about 0.78 - 0.80 $cm^2\,V^{-1}\,s^{-1}$. The discharge gap length d was estimated using the procedure discussed in Appendix A. Therefore, the transit time t_{trans} could be calculated as follows:

$$t_{trans} = \frac{d}{\mu_{ion}\cdot\bar{E}}. \qquad \text{(B2)}$$

REFERENCES

[1] "Toyota Improve hybrid fuel efficiency by 10% with SiC Inverter," http://www.electric-vehiclenews.com/2014/05/toyota-improve-hybrid-fuel-efficiency.html, 2014

[2] J. A. Rosero, J. A. Ortega, E. Aldabas, L. Romeral, "Moving towards a more electrical aircraft," IEEE Aerospace and Electronic Systems Mag., vol. 22, pp. 3-9, 2007.

[3] G. Pietrini, D. Barater, G. Franceschini, P. Mancinelli and A. Cavallini, "An open problem for More Electrical Aircraft (MEA): How insulation systems of actuators can be qualified?," in *Proceedings of the IEEE Energy Conversion Congress and Exposition,* 2016, pp. 1-8.

[4] Partial discharge free electrical insulation systems (Type I) used in rotating electrical machines fed from voltage converters - Qualification and quality control tests, IEC 60034-18-41 ed. 1, Rotating electrical machines – Part 18-41: 2014.

[5] P. Mancinelli, S. Stagnitta and A. Cavallini, "Qualification of Hairpin Motors Insulation for Automotive Applications," IEEE Trans. Ind. Appl., vol. 53, pp. 3110-3118, 2017.

[6] A. Küchler, *High Voltage Engineering – Fundamentals, Technology, Applications,* Springer Vieweg, 2017.

[7] P. Wang, A. Cavallini, G. C. Montanari and G. Wu, "Effect of rise time on PD pulse features under repetitive square wave voltages," IEEE Trans. Dielectr. Electr. Insul., vol. 20, pp. 245-254, 2013.

[8] P. Morshuis, "Assessment of dielectric degradation by ultrawide-band PD detection," IEEE Trans. Dielectr. Electr. Insul., vol. 2, pp. 744-760, 1995.

[9] Electrical measurement of partial discharges (PD) under short rise time and repetitive voltage impulses, IEC TS 61934, Electrical insulating materials and systems 2011.

[10]

[11] D. Fabiani, A. Cavallini and G. C. Montanari, "A UHF Technique for Advanced PD Measurements on Inverter-Fed Motors," IEEE Trans. Power Electronics, vol. 23, pp. 2546-2556, 2008.

[12] N. Hayakawa and H. Okubo, "Lifetime characteristics of nanocomposite enameled wire under surge voltage application [Feature article]," IEEE Electr. Insul. Mag., vol. 24, pp. 22-27, 2008.

[13] A. Cavallini, L. Lusuardi, D. R. Meyer, S. Machipeddy, Modelling partial discharge inception in magnet wires at different altitudes, in *Annual Report Conference on Electrical Insulation and Dielectric Phenomena,* 2016.

[14] L. Niemeyer, "A Generalized Approach to Partial Discharge Modeling," IEEE Trans. Dielectr. Electr. Insul., vol. 2, pp. 510-528, 1995.

[15] D. Fabiani, G. C. Montanari, A. Cavallini and G. Mazzanti, "Relation between space charge accumulation and partial discharge activity in enameled wires under PWM-like voltage waveforms," IEEE Trans. Dielectr. Electr. Insul., vol. 11, pp. 393-405, 2004.

[16] W. Pfeiffer and M. Paede, "About the influence of the frequency on the partial discharge characteristics of enameled wires," in *Proceedings of the Electrical Insulation Conference and Electrical Manufacturing & Coil Winding Conference*, 1999, pp. 485-488.

[17] M. Portnoff, "Time-frequency representation of digital signals and systems based on short-time Fourier analysis," IEEE Trans. Acoustics, Speech, and Signal Processing, vol. 28, pp. 55-69, 1980.

[18] A. Cavallini, A. Contin, G. C. Montanari and F. Puletti, "Advanced PD inference in on-field measurements. I. Noise rejection," IEEE Trans. Dielectr. Electr. Insul., vol. 10, pp. 216-224, 2003.

[19] R. Bartnikas and J. P. Novak, "On the spark to pseudoglow and glow transition mechanism and discharge detectability," IEEE Trans. Dielectr. Electr. Insul., vol. 27, pp. 3-14, 1992.

[20] Phelps Database from LXcat, http://www.lxcat.net/, Accessed: 2016-06-13.

[21] L. Lusuardi, A. Cavallini, P. Mancinelli, G. M. De La Calle, J. M. Martinez-Tarifa, G. Robles, "Design criteria for inverter-fed Type 1 motors", in *Proceedings of the IEEE International Conference on Dielectrics,* 2016, pp. 605-608.

[22] W.O. Schumann, Über das Minimum der Durchbruchfeldstärke bei Kugelelektroden, Archiv für Elektrotechnik, vol. 12, pp. 593-608, 1923. (in German)

[23] E. Kuffel, W. S. Zaengl, and J. Kuffel, *High voltage engineering – Fundamentals,* Oxford, U.K.: Newnes, 2000.

[24] N. H. Malik, "Streamer Breakdown Criterion for Compressed Gases," in IEEE Electr. Insul. Mag., vol. 16, pp. 463-467, 1981.

[25] Kaji, T., Amano, Y., and Asai, H., "Analysis of Influence Factors for Partial Discharge Inception Voltage between Magnet-Wires on Rotating Machines," SAE Technical Paper 2016-01-1226, 2016.

[26] J. Dutton, "A Survey of Electron Swarm Data," J. Phys. Chem. Ref. Data, 4, 681, 1975.

Doris Ragna Meyer was born in 1992 and received the Master's degree in Energy Science and Technologies from the Swiss Federal Institute of Technology (ETH-Z) in 2016. She now works as researcher and technology manager for the on-load tap-changer company Maschinenfabrik Reinhausen (MR), Regensburg, Germany. Her research interests include the physics and measurement of partial discharges, the reliability of electrical systems, the physics of high voltage interruption in vacuum and alternative insulation materials.

Luca Lusuardi (MS'16) was born on 16 September 1991. He received the M.S. degree in energy enegineering from the University of Bologna (Italy) where is currently pursuing the Ph.D. degree in biomedical, electrical and systems engineering. His research interests are diagnosis of insulation systems by partial discharge analysis and reliability of inverter-fed low voltage motors.

Andrea Cavallini (M'95) was born on 21 December 1963. He received from the University of Bologna the Master degree in electrical engineering in 1990 and the Ph.D. degree in electrical engineering in 1995. He was a researcher at Ferrara University from 1995 to 1998. Since 1998, he is an Associate Professor at Bologna University. He was cofounder of spinoff company Techimp HQ Spa. His research interests are diagnosis of insulation systems by partial discharge analysis, reliability of electrical systems and artificial intelligence. He is author or coauthor of more than 250 international papers, and holds 16 international patents.

Davide Barater (S'11-M'14) was born in Italy on August 13, 1983. He received the Master's degree in Electronic Engineering in 2009 and the Ph.D. degree in Information Technology in 2014 from the University of Parma Italy. He was an honorary scholar at the University of Nottingham, U.K., during 2012, and a visiting researcher at the University of Kiel, DE in 2015. He is currently working as research fellow at Department of Engineering and Architecture, University of Parma, Italy. His research area is focused on power electronics for renewable energy systems and motor drives. He is author or coauthor of more than 50 international papers, and holds one international patent.

Alessandro Soldati got his B.Sc. and M.Sc. degrees in 2011 and 2013 respectively, from the University of Parma. After spending some time in an industrial-truck equipment company, he attended the PhD course in Information Engineering, at the same University. He is discussing his thesis in 2018. He is now a research assistant working on electric powertrains. His research interests focus on active gate drivers for wide band-gap devices, high-density power converters and motor control algorithms. He is also CTO of eDriveLAB, a spin-off company in vehicle electrification, and author of one patent.

Giorgio Pietrini received the B.Sc. and M.Sc. degrees from the Department of Information Engineering at University of Parma, Italy, in 2009 and 2014 respectively. He is now pursuing the Ph.D. degree in Information Technology at the same university. His research interests include electrical machine modeling and design with special regard to permanent magnet synchronous motors for high performance automotive traction applications.